Supercontinuum lidar applications for measurements of atmospheric constituents

David M. Brown, Zhiwen Liu, C. Russell Philbrick
The Pennsylvania State University Department of Electrical Engineering,
University Park, PA USA 16802

ABSTRACT

Recent advances in the field of supercontinuum lasers have provided a unique opportunity for developing lidar instruments that cover a wide spectral range. These instruments permit many simultaneous measurements of differential absorption spectra (DIAL and DAS techniques) to determine species density. Application of MODTRAN^{TM} 5 and other simulation software has allowed us to design and validate the findings of supercontinuum lidar systems developed at Penn State Lidar Laboratory. The multiple line differential absorption concepts have been demonstrated with various system topologies for a host of atmospheric windows in the visible to near infrared regions. During the past three years, we have developed and demonstrated several systems that are capable of measuring concentrations of various atmospheric constituents at background or elevated levels through long path absorption by transmitting only milliwatts of optical power. Our most recent supercontinuum lidar system utilizes a nanosecond supercontinuum laser fiber optically coupled to a transceiver system for remote sensing of atmospheric species concentrations. Due to the flexibility of the design, the operational prototype is currently being used to demonstrate the capability for accurately measuring real world open path atmospheric concentrations across the Penn State campus. The purpose of this study is to develop the technology and to demonstrate the capability for accurately measuring species concentrations without the complexities and uncertainties inherent in hyper-spectral remote sensing using the sun as a source, or the limitations and errors associated with using pairs of laser lines for DIAL measurements of each species. Initial simulations and measurements using this approach are presented.

Keywords: Supercontinuum laser, lidar, DIAL, MODTRAN, differential absorption

1. INTRODUCTION

The wide spectral bandwidth provided by relatively low cost, stable supercontinuum sources allows development of remote sensing applications that can utilize large spectral regions of the visible and NIR regions of the electromagnetic spectrum. The Supercontinuum Absorption Lidar system (SAL) at Penn State was created by combining robust multiple wavelength data processing algorithms with the broad spectral bandwidth and laser like characteristics of supercontinuum sources. The broadband spectral return information offered by the system provides the capability to map the absorption of many different molecules with overlapping absorption spectra simultaneously present in atmosphere. The techniques provide rapid, highly robust measurements of atmospheric constituents at background levels and will be expanded for plume mapping of localized regions, and high sensitivity long range path averaged measurements.

By using arbitrary comparison line selection over a broad spectral region, the Supercontinuum Absorption Lidar (SAL) is not tied to the DIAL paradigms of a limited number of laser line pairs, or by the requirement of computing the ratios of nearby wavelength pairs because of broadband spectral bias effects. Instead, the SAL approach samples the spectral region of interest at many wavelengths to determine not only the concentration of the species of interest, but also provides information on any background spectral bias effects. Additionally, by acquiring all the spectral information of absorption at one time, interference and disturbance attributed to atmospheric turbulence and target speckle can be more efficiently managed. Therefore, the probability of correct detection and inversion in high speed applications is increased with SAL approaches when compared to other atmospheric measuring technologies.

Laser Radar Technology and Applications XIII, edited by Monte D. Turner, Gary W. Kamerman
Proc. of SPIE Vol. 6950, 69500B, (2008) · 0277-786X/08/$18 · doi: 10.1117/12.778255

2. SUPERCONTINUUM ABSORPTION LIDAR (SAL) APPROACH TO ATMOSPHERIC GAS DETECTION

1.1 SAL Hardware description

The Supercontinuum Absorption Lidar (SAL) utilizes a combination of techniques developed for Differential Optical Absorption Spectroscopy (DOAS) and Differential Absorption Lidar (DIAL) systems. The system developed at the Department of Electrical Engineering at Penn State has been tested using long path absorption between rooftops on the campus. Two configurations were used to determine the performance of the existing hardware as a function of operational distance. The first configuration places the supercontinuum source and the detection spectrometer on the building rooftop at the location of the transceiver optics. This was initially used to observe water vapor on a 280 m path to maximize the return signal to the optical spectrum analyzer being used to interpret the return. The second configuration fiber-optically couples the source and detector to an optical laboratory in the basement of the building where a high resolution liquid nitrogen cooled detector is used to measure the return signal. In this configuration, the system can be used in a general purpose manner for detection of several atmospheric constituents due to the increased sensitivity of the detector, and stability of the supercontinuum source. In both configurations, the source in the lidar transceiver, which is described in more detail in subsequent sections of this report, is a low power supercontinuum laser built in our optical laboratory from commercial off-the-shelf parts. After being properly collimated, the supercontinuum beam is expanded to reduce the amount of far field diffraction and steered to a remote retroreflector target. Since the transmitted beam and the telescope are on the same optical axis, and the source and collection instruments are either at the same location, or fiber-optically coupled to the transceiver optics, we are able to simply point the system at remote targets without the need of constant realignment. The return from the retroreflector target passes the turning mirror used to turn the transmitted beam into the transmit path and is then collected using a four inch Newtonian telescope. The light is focused into a collection fiber that is directed into a portable optical spectrum analyzer under the first configuration, and into a 50 m fiber that directs the return to a remote high resolution spectrograph under the second configuration. Following the spectral analysis of the return by one of the spectrometer options, the data is processed by numerous data analysis routines described in subsequent sections of this work.

Shown below in Figure 1(a) is a version of the first configuration used to make water vapor measurements over a ~280 m total two way path between the EE East building (labeled EEE) and the Dieke building (labeled DKE) shown in Figure 1(c). Under this initial measurement condition, a mirror was not used to double the total path length as it was in later experiments. Instead, the retroreflector was positioned on the roof of the Dieke building and aligned with the system as shown by Figure 1(b). Later experiments invoked the use of a mirror on the Dieke building and a retroreflector on the EE East building to test the performance of the system when operating with a 540 m total two way path length as shown by Figure 1(c).

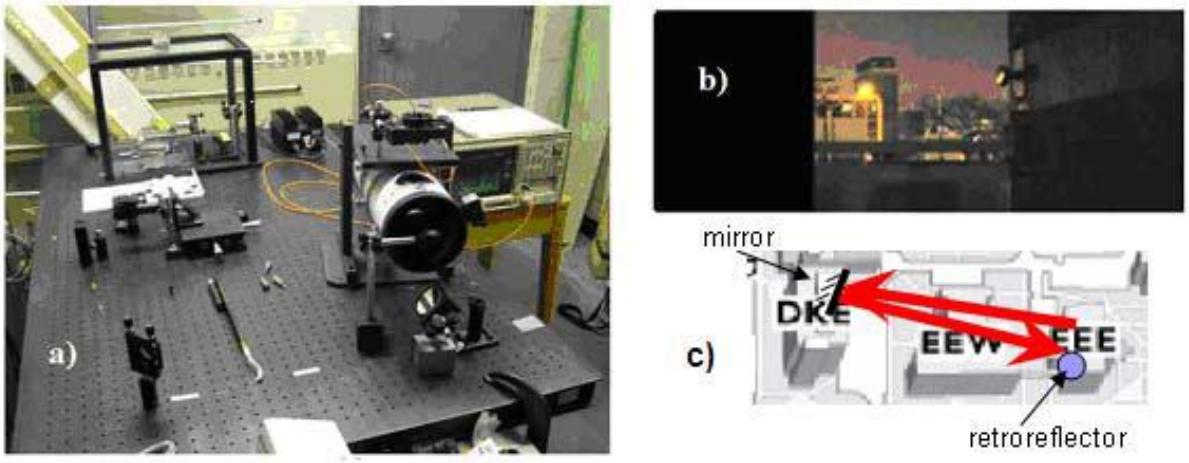

Fig. 1. (a) Initial configuration of SAL hardware to make first atmospheric path measurement of water vapor concentration, (b) supercontinuum backscatter from retroreflector target under operation, and (c) later atmospheric path configuration used to increase the total two way path length of beam.

Initial supercontinuum SAL investigations took and continue to take advantage of the proven multi-wavelength approaches developed for hyperspectral remote sensing, but add the capability to confine the illuminating source. The SAL transmitter in our system utilizes a laboratory built, low power, relatively low cost supercontinuum source. By coupling sub-nanosecond laser pulses from a passively Q-switched microchip laser (JDSU NP-10620-100, wavelength at 1064 nm, average power ~ 40 mW) into a 20 m photonic crystal fiber (Blaze Photonics SC-5.0-1040) we are able to generate supercontinuum white light 0. Four wave mixing is the primary mechanism responsible for the creation of broadband laser light using this approach. A typical spectrum of the supercontinuum source used for absorption investigations begins near 500 nm and extends into the near infrared beyond 1600 nm. The spectral signature of the source fills the range shown in Figure 2 based on measurements by an Ando (now Yokogawa) optical spectrum analyzer (AQ6315E).

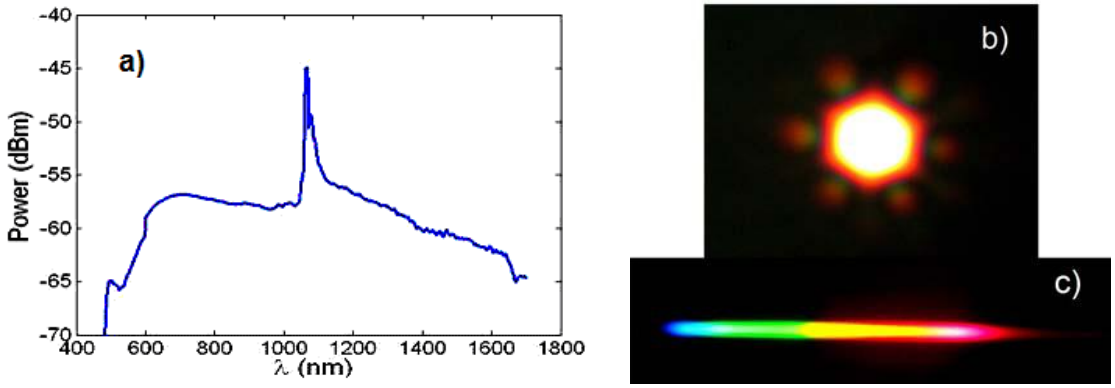

Fig 2. (a) Supercontinuum source spectrum (b) The far field pattern of the supercontinuum spectrum generated from a photonic crystal fiber. (c) The rainbow observed after the collimated light passes through a prism.

The high spatial coherence and broad bandwidth of the supercontinuum source makes it possible generate an ideal broad-band source. The supercontinuum output of the beam profile from the photonic crystal fiber is shown in Figure 2(b). If the collimated supercontinuum light passes through a grating, a rainbow is formed, see Figure 2(c). It is the broad bandwidth and high spatial coherence characteristics of the supercontinuum source that are particularly interesting for remote sensing applications.

1.2 Data processing and interpretation

To properly interpret the SAL return information, it is important to select a data processing approach that is able to sample the spectral return information and use as many wavelengths as possible to determine a final target species concentration. We tested several algorithms ranging from simple least square fitting to more complex maximum likelihood estimation techniques, and found that MLE techniques are most useful for interpreting SAL return information due to the random nature of the noise present in the signal. We speculate that there are multiple reasons for the "high frequency" nature of the noise including atmospheric turbulence, variation in the transmission as a function of wavelength for different optical modes in the receiving and transmitting fibers, aerosol scattering, and statistical noise of the collected optical signal. In addition to impressive ability of the MLE approach to fight various sources of noise in the spectral return, the selected MLE data processing approach is able to estimate the concentration of several target species with overlapping absorption spectra. Before the algorithm is applied however, it is important to adjust the spectral absorption features for each of the possible target species to a resolution similar to the collected data. If the effective slit width is not matched the analysis will yield concentrations for each target species that are heavily biased. We found through experimentation that good agreement is achieved by either matching the slit width of the experimental measurement, or by re-sampling the collected dataset with a wider effective slit width and using the appropriate calculation of spectral absorption features.

To test the performance of the developed data analysis approach, we have selected a region in the near infrared that has spectrally overlapping absorption structure of CO_2, CH_4, and H_2O and simulated a broadband SAL spectral return. For general applications and flexible simulations, cross section data are calculated from HITRAN intensity datasets by following well developed equations for pressure and temperature broadening 0. Figure 3 shows the calculation result of temperature and pressure broadening of the HITRAN intensity datasets for the spectral region of interest. These spectra are one of the main inputs to the MLE data processing step.

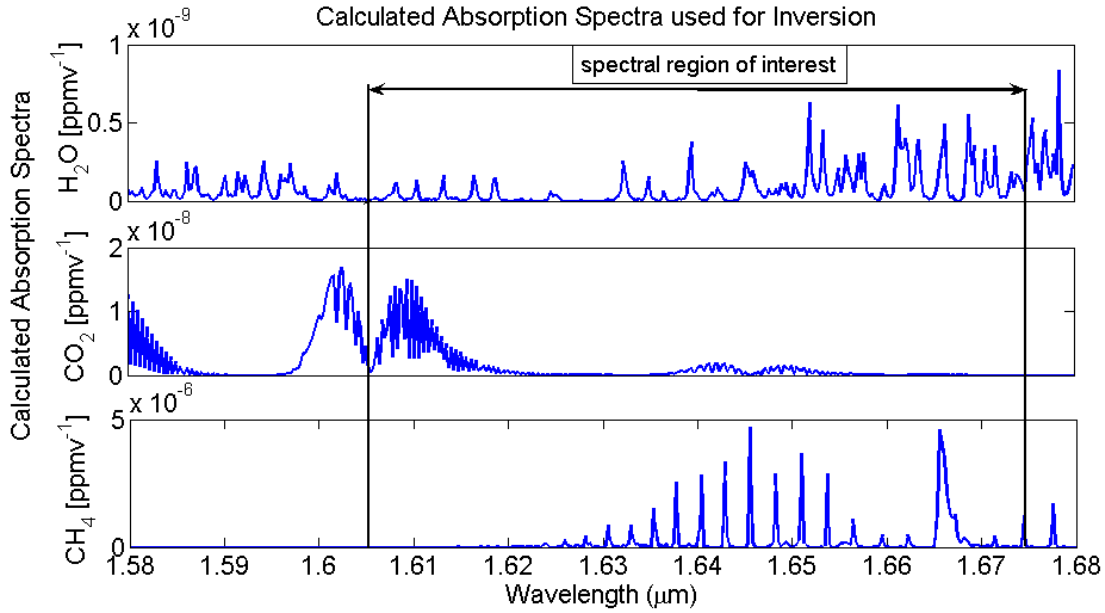

Fig 3. Spectral absorption data of H_2O (upper), CO_2 (middle) and CH_4 (lower) calculated using standard temperature and pressure.

After the absorption spectra have been calculated, we simulate a SAL return using MODTRAN™4 0with a signal to noise ratio equation for differential absorption measurements, a one kilometer length path length, and typical atmospheric concentrations of each of the target species. The signal to noise ratio equation allows us to introduce random fluctuations as a function of wavelength that approximates those fluctuations observed with our initial atmospheric path measurements. The typical equation for DIAL SNR normalized and modified for multiple targets in terms of the spectral return power is shown below as equation (1) 0.

$$SNR_{total} = \left[2\left[\left(\frac{\sigma_{P_{off}^{T1}}}{< P_{off}^{T1} >} \right)^2 + \left(\frac{\sigma_{P_{on}^{T1}}}{< P_{off}^{T1} > - P_{\Delta}^{T1}} \right)^2 \right]^{-1} + 2\left[\left(\frac{\sigma_{P_{off}^{T2}}}{< P_{off}^{T2} >} \right)^2 + \left(\frac{\sigma_{P_{on}^{T2}}}{< P_{off}^{T2} > - P_{\Delta}^{T2}} \right)^2 \right]^{-1} + \ldots \right]^{1/2} \quad (1)$$

Here, $< P_{off}^{T1} > - P_{\Delta}^{T1} =< P_{on}^{T1} >$, and $< P_{off}^{T1} >$ is denoted as the average optimal off line return for target 1 with variance $\sigma_{P_{off}^{T1}}$, $< P_{on}^{T1} >$ is denoted as the average optimal on line return for target 1 with variance $\sigma_{P_{on}^{T1}}$, and P_{Δ}^{T1} is denoted as the peak-to-peak differential power received for target 1 specified by the appropriate DIAL wavelengths. Since we are deriving a total signal to noise classifier for multiple targets using many wavelengths in a specified inversion band, we use the largest peak-to-peak differential power in the band for each target to specify P_{Δ}^{T1}. While this value will vary for different spectral ranges due to absorption strength and concentration of the target species, it provides a way to track the performance of the MLE analysis algorithm as the targets SNR is reduced and the random fluctuations approach and peak to peak differences in the noiseless spectral return. We then add the normalized SNRs for each of the targets present in quadrature to determine a total SNR. To utilize Eq. 1 to add spectral noise to simulated SAL return created by MODTRAN™ 4 in terms of total SNR, we set $< P_{off} >$ equal to 1, and assume that the online and offline variance for each of the targets is the same. Shown below in Figure 4 are the normalized simulated SAL returns operating under different SNR cases. The top plot corresponds to case where there is no noise, while the middle and lower plots correspond to low and high SNR cases.

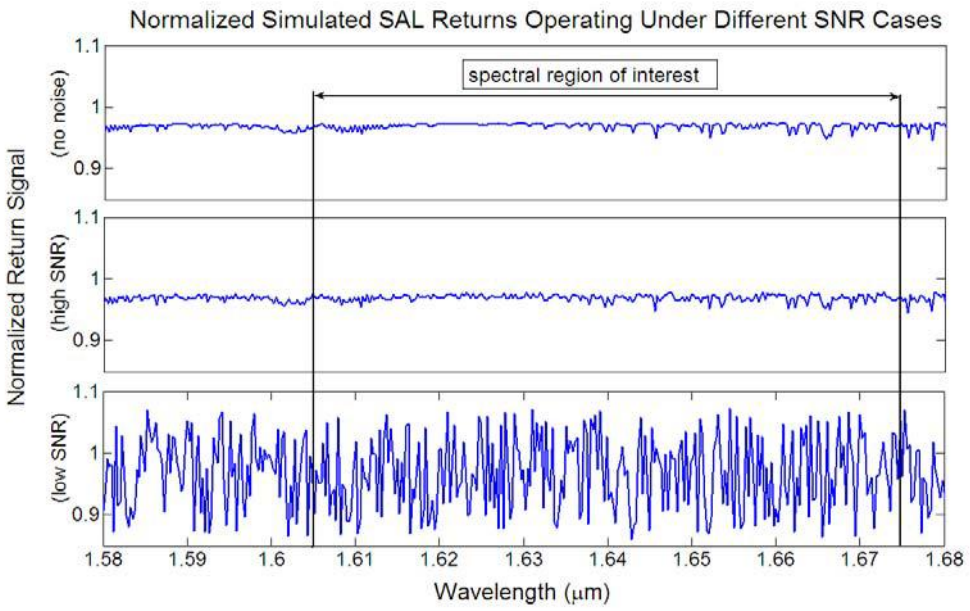

Fig. 4. Simulated return calculated for 23 km visibility along a 1 km path length under different SNR cases.

The approach used to process the SAL data is a version of the algorithm originally developed by Warren 0 and was later simplified by Yin and Wang 0. The changes made by Yin and Wang make the algorithm more robust to noise details by estimating a CPL using a weighted sum of all absorption cross section features sampled instead of looking at individual samples. This change prevents the algorithm from arriving at a CPL estimation that will later grow without bound due to a bad set of data points. By starting with an initial CPL guess and spectral return information, the algorithm simultaneously solves for the noise covariance matrix, $\hat{\Lambda}$, and CPL of multiple vapors. This process uses a complete array of wavelength specific target vapor absorption parameters, α, simulated signals, $\hat{H}$, and average SAL returns, $\overline{Q}(j)$ (see Eq. 2 main parenthesized component) 0. After a number of iterations, the result will approach an estimated CPL for each target, l, if the target is present in the collected information. As shown by Eq. 2, we utilize the MLE algorithm as core data processing step for the approach used in conjunction with the SAL data.

$$CPL_l = \frac{1}{n-1}\sum_{M=2}^{n}\left[\frac{\sum_{j=1}^{M}\left[\alpha_{jl}\hat{\Lambda}_1^{-1}(j,j)\left[\hat{H}_1 - \overline{Q}(j) - \sum_{l=1,l\neq 1}^{L}\alpha_{jl}CPL_l\right]\right]}{\sum_{j=1}^{M}\left[\alpha_{jl}\hat{\Lambda}_1^{-1}(j,j)\alpha_{jl}\right]}\right]\left[ppm\cdot m\right] \qquad (2)$$

To further increase the robustness of the CPL result, we use the MLE to calculate a CPL result as we increase the number of sample wavelengths from two to several hundred since we have many wavelengths for selection in most molecules. We then use a Hamming window to smooth this result and examine the CPL conclusion for the last hundred wavelength comparisons. By doing this we are able to reduce the standard deviation in the final CPL result and increase the level of confidence in the result of the estimated concentration of the target gas or gases. To demonstrate the performance of the MLE algorithm, the number of wavelengths used is increased, and we plot the normalized percent difference from the expected concentration and the normalized percent variation in this concentration for the concluded CPL for each of the three target gases in Figure 5. We have performed this analysis for two different signal to noise ratio cases, one with a SNR of 4 and one with a SNR of 10 using Eq. 1. As we increase the number of wavelengths used for comparison, the accuracy of detection for H_2O and CH_4 is low using few lines due to the low absorption character of these species in this region. Furthermore, the inversion of CO_2 is not highly accurate due to the interference of noise and spectral bias from closely spaced wavelengths. However, as the number of wavelengths is increased, the detection performance improves dramatically for each of the target species. From these results it is clear that species detection

from SAL return data on base of MLE inversion with enough lines has good performance even at relatively low signal to noise ratios.

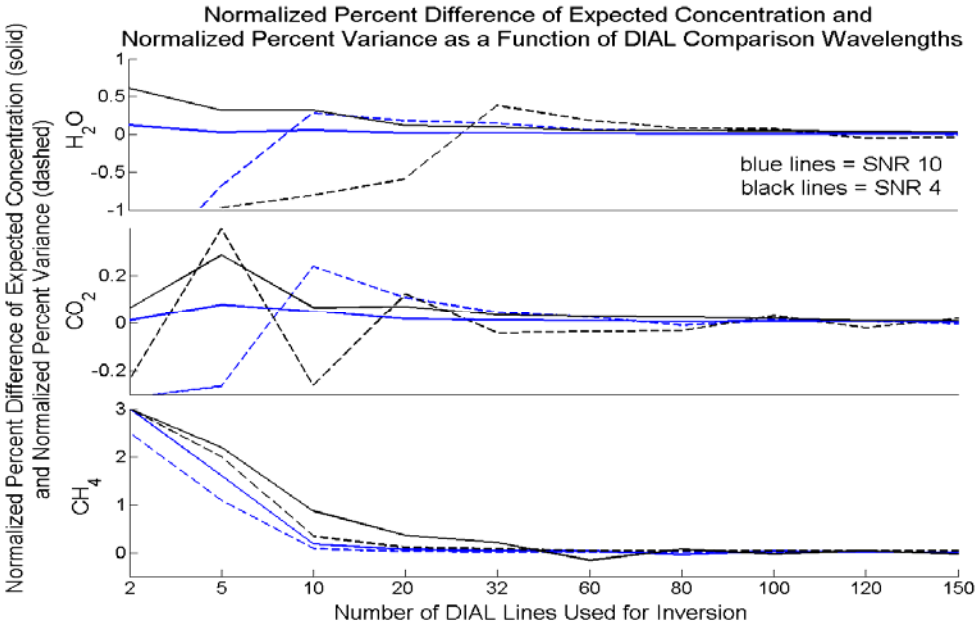

Fig. 5. The normalized percent difference from the expected concentration (blue lines) and normalized percent variation (black lines) are plotted as a function of the number of DIAL lines used for comparison under a SNR case of 4 (dashed line) and 10 (solid line).

3. EXAMINATION OF ABSORBING SPECIES WITH BROAD STRUCTURE

Various studies were performed with the SAL to examine the ability to measure concentrations of atmospheric water vapor. These studies included a 20 m laboratory path measurement to test the performance of the developed MLE algorithm, and multiple ~300 m atmospheric path measurements where simpler least square fitting algorithms were tested for performance benchmarks. These initial measurements provided a clear method for developing the techniques required to measure other absorbing species. A summary of the water vapor measurements is presented in this section.

Figure 6 shows the result of an indoor 20 m atmospheric path measurement of water vapor matched with the appropriate MODTRAN^{TM} simulation result. The MLE algorithm estimation of the water vapor concentration was used to determine the appropriate concentration of water vapor to enter into the MODTRAN^{TM} simulation and is shown as the right-half of Figure 6. By examining the final iterated CPL values, we are able to conclude that our analysis using up to 500 wavelengths shows the mean detection concentration of water vapor for the 20 m path is relatively constant when more than 50 wavelengths are selected for comparison. This yields a result of 10900 +/- 200 ppm and a 5.8% difference when compared to the value of RH humidity determined from a point measurement within the laboratory. We suspect that the measurement mechanism of the water vapor concentration is somewhat to blame for the difference, as the absorption measurement is a full path average while the laboratory relative humidity meter may have been skewed by a localized region. Additionally, temperature variations in the laboratory due to the HVAC ducts could have further skewed the localized result.

Figure 7 below shows the result of a water vapor absorption measurement using an outdoor 300 m two way path. This measurement utilized the initial SAL configuration (supercontinuum source and detection spectrometer in roof laboratory with transceiver optics) to make the atmospheric measurement. A least square fitting algorithm was used to fit the data to various MODTRAN^{TM} simulations with different values of relative humidity. As shown by the right half of Figure 7, the best fit was for a relative humidity of 62.5% which agreed well with the 63.5% relative humidity measured by a MET station deployed nearby 0.

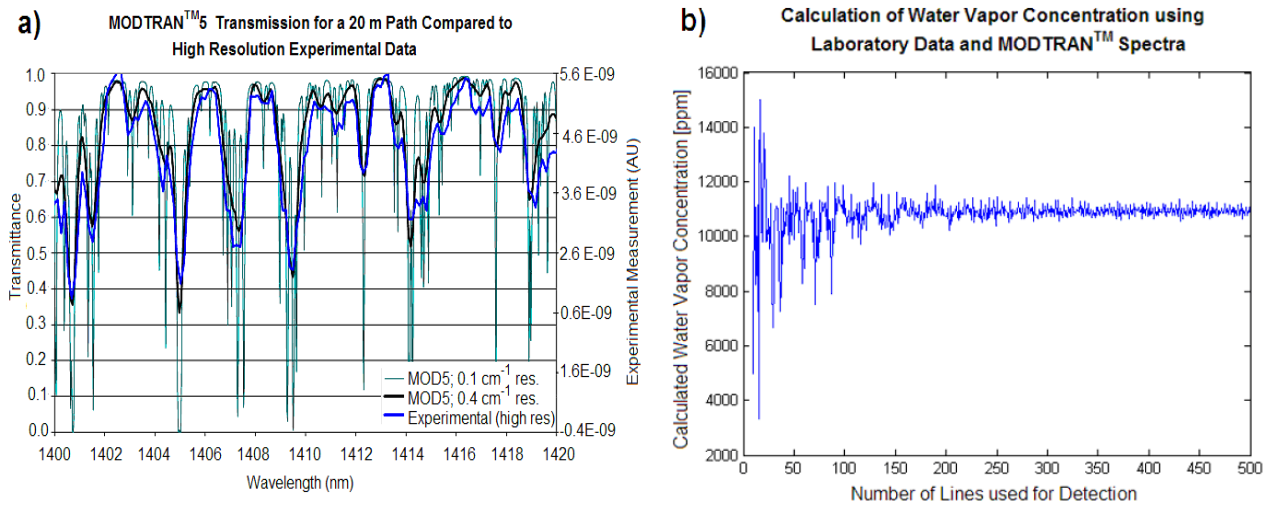

Fig. 6. (a) Spectral scan of the 1400 to 1420 nm band in the infrared for a 20 m laboratory path matched with the appropriate MODTRAN™ result. (b) MLE algorithm was used to determine path concentration of water vapor 0.

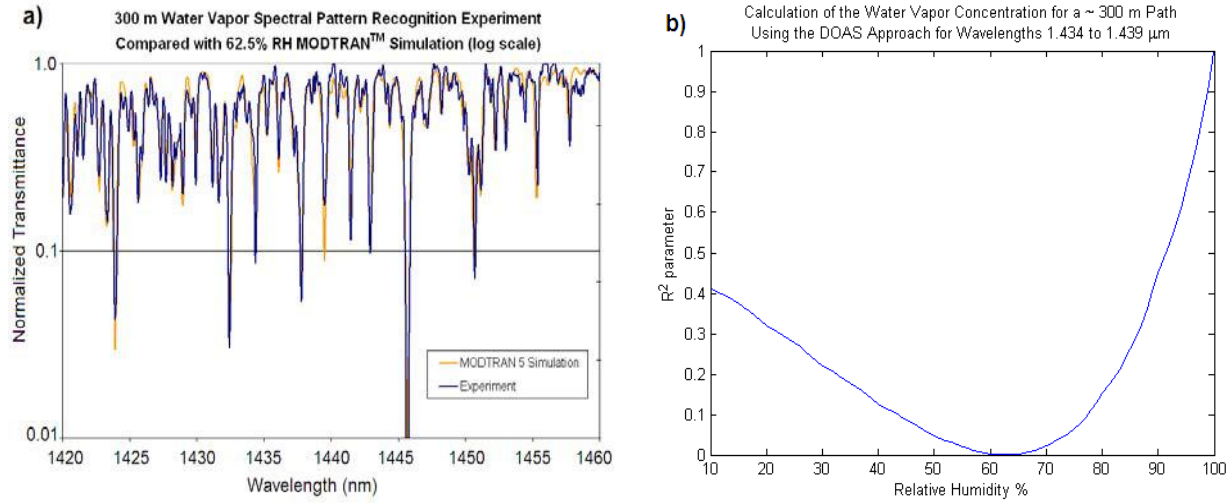

Fig. 7. (a) Spectral scan of the 1420 to 1460 nm band in the infrared for a 300 m atmospheric path matched with the appropriate MODTRAN™ result. (b) Least square fitting of raw data to determine relative humidity concentration throughout path 0.

4. EXAMINATION OF ABSORBING SPECIES WITH FINE STRUCTURE

Various factors influence the strength of the return signal including atmospheric turbulence, laser stability, aerosol concentration, etc. By using the liquid nitrogen cooled detector on our spectrograph, we are able to collect the supercontinuum signals under a variety of environmental conditions that would usually inhibit long path differential absorption measurements due to near complete absorption of the transmitted signal. Additionally, by remotely locating the supercontinuum source in a temperature stabilized laboratory, many of the low frequency wavelength fluctuations in the transmitted beam were reduced. This allowed us to capture many datasets for each absorption measurement without much concern of sources wavelength stability. Figure 8 shows a diagram of the current, general purpose, SAL system configuration being used to make supercontinuum absorption measurements. The system has various quick disconnects for alignment in addition to tightly wound fiber coils before and after the 50 m section between the roof and basement laboratories to "filter" the transmitted and received supercontinuum spectra. An initial problem with the technique

stemmed from the propagation of supercontinuum light down an optical fiber from the roof location to the basement laboratory. Because previous experiments focused on broadband absorption features, we initially observed the supercontinuum spectral return using lower resolution in our spectral instruments and had success in remotely detecting water vapor absorption features. When observing the same regions in high resolution as required for observing oxygen features, we noted relatively large fluctuations in the spectral return – similar in magnitude to the oxygen absorption. We expect these fluctuations are due to the variations in the efficiency of different high order mode propagation in the fibers. This efficiency as a function of wavelength can be calculated knowing specific fiber parameters; however, this would prove to be extremely time consuming given than the supercontinuum spectrum is continuous across the entire absorbing region of interest. Therefore, we employed filters to provide a simple and easy way to allow higher order modes to "leak" from the core-cladding interface. By inhibiting the propagation of higher order modes, the transmission spectrum for the fiber is more constant as a function of wavelength and permits measurements at high resolution to detect species with fine structure.

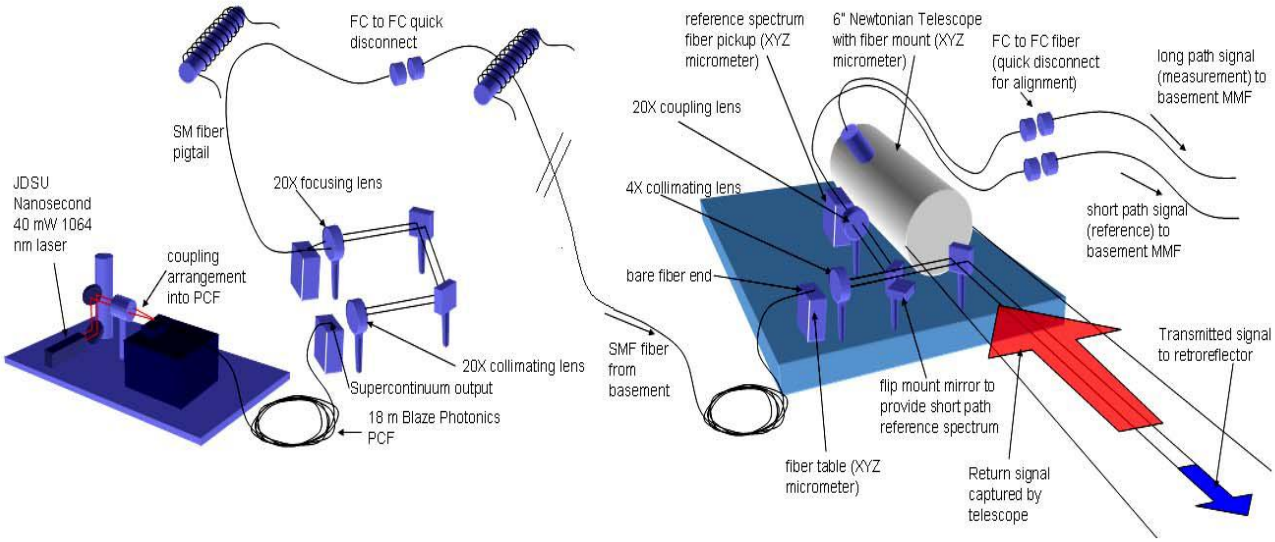

Fig. 8. Supercontinuum absorption lidar using a low power supercontinuum source and detector that are fiber optically coupled to rooftop mounted transceiver system.

Further difficulties with the measurement approach were realized when attempting to match measured SAL return information to the HITRAN calculated cross sections, or MODTRAN™ simulation results in high resolution during analysis of the first set of atmospheric oxygen absorption measurements. Initially, All MODTRAN™ simulations performed in this study were found to be offset from experimental results by roughly 0.2 to 0.3 nm. During the atmospheric water vapor absorption studies, this deviation had gone unnoticed because the spectral match was examined at a far coarser resolution than that required for measurement of atmospheric oxygen. At the 2007 AFRL Transmission Meeting it became apparent that this difference was due to the lack of the conversion of MODTRAN™ output wavelengths from vacuum conditions to those expected in air. When then applying the standard equation for conversion (Eq. 3) to the MODTRAN™ outputs, excellent agreement is realized between normalized SAL return spectra containing oxygen absorption, see Figure 9 0. Wavelengths in Eq. 3 are in nanometers.

$$\lambda_{air} = \frac{\lambda_{vac}}{1.0 + 2.735182\times10^{-4} + \frac{13.14182}{\lambda_{vac}^2} + \frac{2.76249\times10^5}{\lambda_{vac}^4}} \qquad (3)$$

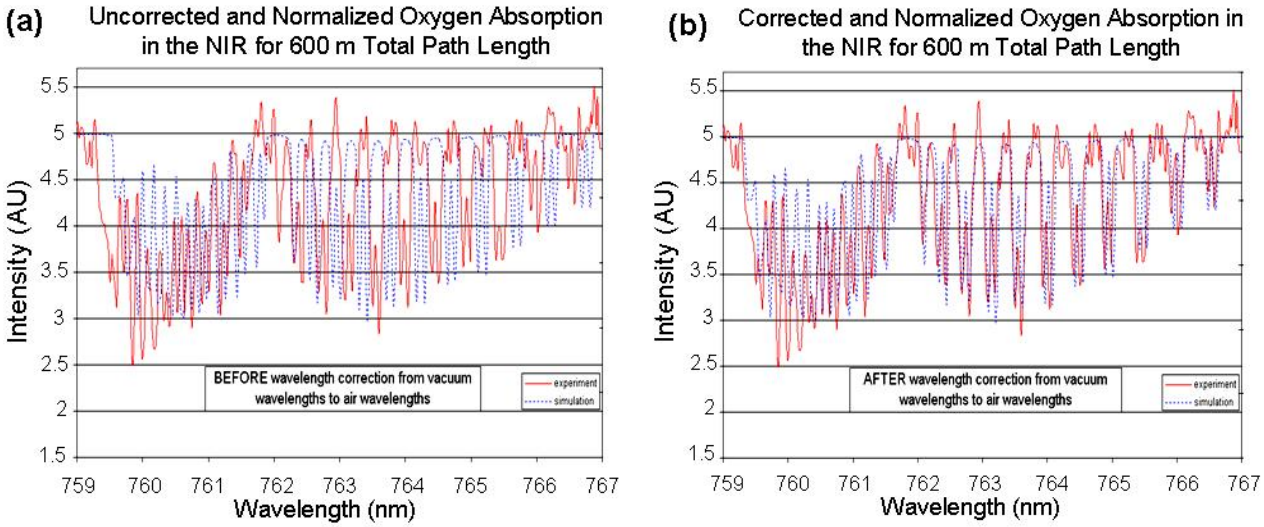

Fig. 9. Uncorrected (a) and corrected (b) MODTRAN™ simulation results are compared with raw experimental data.

Further experimentation with oxygen absorption led to testing the developed MLE algorithm on normalized raw and spectrally smoothed SAL data. Measurements from various datasets showed that although the MLE algorithm resulted in a mean CPL that was reasonably accurate, the error bars on the path integrated measurement were too large. Therefore, the SAL spectral datasets and the calculated HITRAN cross sections were smoothed with a coarser 6.4 cm^{-1} effective slit width resolution. The algorithm initially developed to determine the best effective slit width for smoothing HITRAN simulations was used to confirm the functionality of the calculation and smoothing procedures. The result is shown in Figure 10. The best match or highest correlation coefficient is found only when the inverted HITRAN cross section is compared to the smoothed data with roughly a 6.42 cm^{-1} effective slit width.

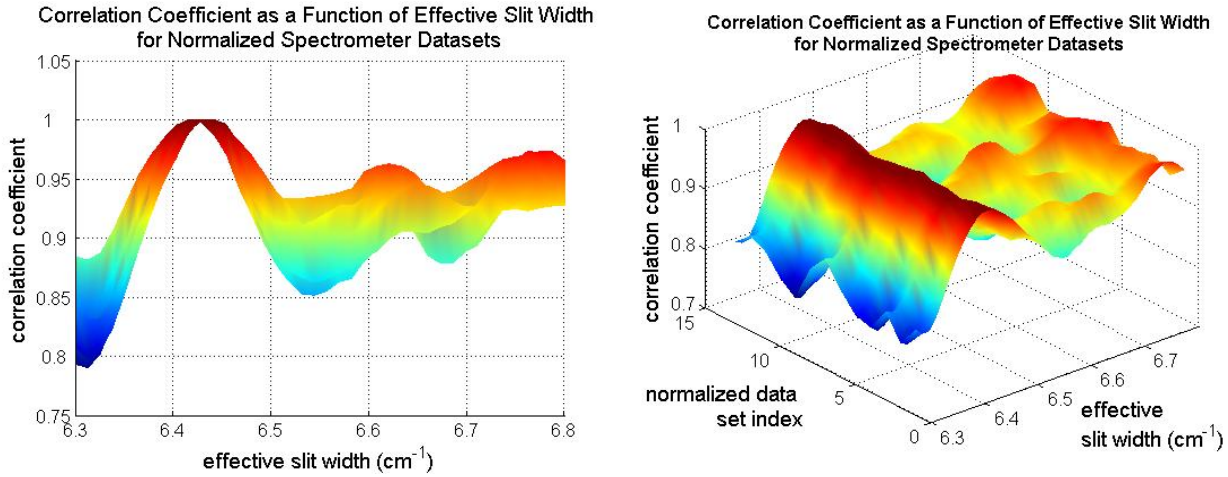

Fig. 10. Calculation of correlation coefficient between smoothed SAL spectral return data and inverted HITRAN cross section as the effective slit width is varied for all datasets captured for a single atmospheric oxygen measurement.

By entering the appropriate slit width and SAL spectral data into the MLE algorithm, we arrive at a mean atmospheric oxygen concentration of 209180 ppm with a standard deviation of 47 ppm as we increase the data processing to included hundreds of wavelengths. We expect that the reason for deviation from the standard atmospheric concentration of oxygen is due to the low resolution of the laser range finder used with the SAL to estimate range to target. With only a 1 m resolution, the range finder can introduce hundreds of ppm error into the measurement of atmospheric oxygen

concentration in this configuration. When the resolution, concentration, and range are properly entered in the MODTRAN™ simulation, striking agreement is observed between the simulated and normalized experimental datasets as shown by Figures 11 and 12.

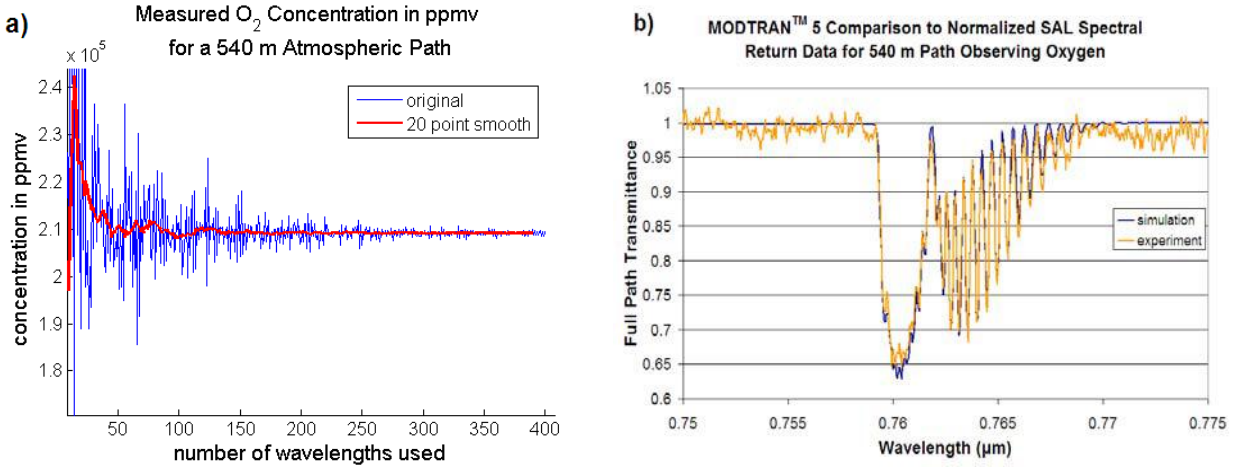

Fig. 11. MLE algorithm result for concentration of oxygen (a), and comparison between experimental and simulated SAL spectra (b).

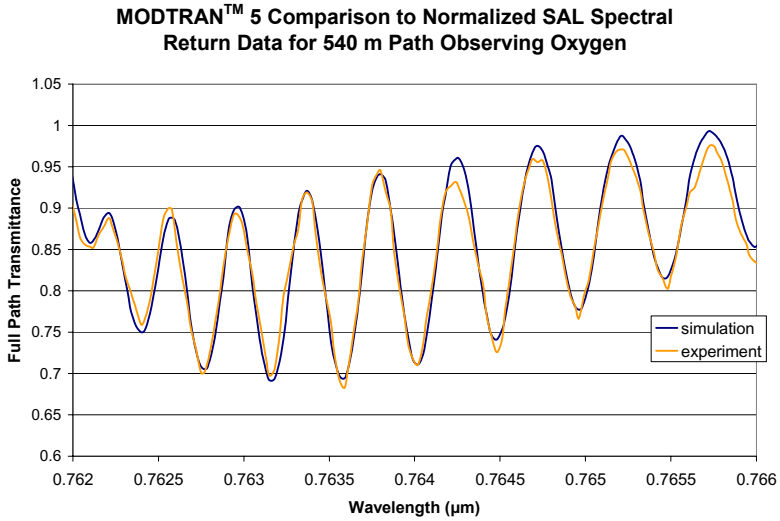

Fig. 12. Zoom of spectral comparison between experimental and simulated SAL spectra.

5. CONCLUSIONS

We have demonstrated a technique that capable of detecting and measuring concentrations of multiple gaseous targets with overlapping absorption spectral features. The algorithms developed in these studies have been tested on simulated and experimental supercontinuum absorption lidar measurements of water, methane, oxygen, and carbon dioxide. The performance of the SAL approach varies, and depends on careful data processing, the strength of the absorption structure and total path length of interest. Future work will strive to extend the supercontinuum into the NIR and eventually the MWIR to take advantage of the large cross sections for many hydrocarbons that lie there.

With pollution levels continually increasing and causing more concerns, an accurate and robust method for measurement is a necessity to asses the impact of humans on the environment. For such a technique to be successful, it must be able to be implemented for a wide range of applications. With the ability to survey areas from city blocks to entire towns for many airborne molecular species using a large wavelength range, the SAL technique has many future

applications. The ultimate urban remote sensing system would be a device capable of producing highly accurate 2D mapping capability for a range of airborne molecular species. The market segment for such a device includes use for emergency response or natural disaster scenarios. The developed approach can accomplish this task with multiple path supercontinuum absorption measurements over a selected area. We envision such systems implemented in many of the large cities of the world in the future for daily monitoring of pollution levels with the added capability of emergency monitoring chemical or biological threats to the population.

REFERENCES

[1] Alfano, R.R., *Supercontinuum Laser Source*, Springer Verlag, New York (1989).

[2] Rothman, L.S., C. P.Rinsland, A. Goldman, S.T. Massie, D.P. Edwards, J. M. Flaud, A. Perrin, C. Camy-Peyret, V. Dana, Y. Mandin, J. W. Schroeder, R.R Gamache, R.B. Wattson, K. Yoshino, K.V. Chance, K.W. Jucks, L.R. Brown, V. Nemtchinov, P. Varanasi, " The HITRAN Molecular Spectroscopic Database and HAWKS (HITRAN Atmospheric Workstation): 1996 edition," J. Quant. Spectro. Rad. Transfer 60(5), 665-710 (1998).

[3] Berk, A., T.W. Cooley, G.P. Anderson, P.K. Acharya, L.S. Bernstein, L. Muratov, J. Lee, M.J. Fox, S.M. Adler-Golden, J.H. Chetwynd, M.L. Hoke, R.B. Lockwood, J.A. Gardner, P.E. Lewis, "MODTRAN5: A reformulated atmospheric band model with auxiliary species and practical multiple scattering options," in Algorithms and Technologies for Multispectral, Hyperspectral, and Ultraspectral Imagery X, Proc. SPIE 425, 341-347 (2004).

[4] Brown, D.M., A. Willitsford, K. Shi, Z. Liu and C.R. Philbrick, "Advanced Optical Techniques for Measurements of Atmospehric Constituents," in *Proc. 28th Ann. Rev. Atmos. Trans. Models*, Lexington MA, June (2006).

[5] Warren, R.E., "Optimum detection of multiple vapor materials with frequency-agile lidar," Appl. Opt. 35, 4180-4193 (1996).

[6] Yin, S., and W. Wang, "Novel algorithm for simultaneously detecting multiple vapor materials with multiple-wavelength differential absorption lidar," Chin. Opt. Lett. 4, 360-362 (2006).

[7] Brown, D.M., K. Shi, Z. Liu, C.R. Philbrick, "Advanced Optical Techniques for Measurements of Atmospheric Constituents," submitted for publication to Optics Express (2008).

[8] Morton, Donald C. "Atomic data for resonance absorption lines. I - Wavelengths longward of the Lyman limit" Astrophysical Journal Supplement Series (ISSN 0067-0049) 77, 119-202 (1991).